Phosphorylation-induced torsion-angle strain in the active center of HPr, detected by NMR and restrained molecular dynamics refinement

Nuland, Nico A.J. van; Wiersma, Jonna A.; Spoel, David van der; Groot, Bert L. de; Scheek, Ruud M.; Robillard, George T.

Published in:
Protein Science

DOI:
10.1002/pro.5560050305

Protein Science (1996), *5*:442–446. Cambridge University Press. Printed in the USA.

Phosphorylation-induced torsion-angle strain in the active center of HPr, detected by NMR and restrained molecular dynamics refinement

NICO A.J. VAN NULAND,[1] JONNA A. WIERSMA,[2] DAVID VAN DER SPOEL,[2] BERT L. DE GROOT,[2] RUUD M. SCHEEK,[2] AND GEORGE T. ROBILLARD[2]

[1] New Chemistry Laboratory, University of Oxford, South Parks Road, OX1 3QT Oxford, United Kingdom
[2] Groningen Biomolecular Sciences and Biotechnology Institute, and the Department of Biochemistry and Biophysical Chemistry, University of Groningen, Nijenborgh 4, 9747 AG Groningen, The Netherlands

(RECEIVED October 2, 1995; ACCEPTED December 13, 1995)

Abstract

The structure of the phosphorylated form of the histidine-containing phosphocarrier protein HPr from *Escherichia coli* has been solved by NMR and compared with that of unphosphorylated HPr. The structural changes that occur upon phosphorylation of His 15, monitored by changes in NOE patterns, $^3J_{NHH\alpha}$-coupling constants, and chemical shifts, are limited to the region around the phosphorylation site. The His15 backbone torsion angles become strained upon phosphorylation. The release of this strain during the phosphoryl-transfer to Enzyme II facilitates the transport of carbohydrates across the membrane.

From an X-ray study of *Streptococcus faecalis* HPr (Jia Z, Vandonselaar M, Quail JW, Delbaere LTJ, 1993, *Nature 361*:94–97), it was proposed that the observed torsion-angle strain at residue 16 in unphosphorylated *S. faecalis* HPr has a role to play in the protein's phosphocarrier function. The model predicts that this strain is released upon phosphorylation. Our observations on *E. coli* HPr in solution, which shows strain only *after* phosphorylation, and the fact that all other HPrs studied thus far in their unphosphorylated forms show no strain either, led us to investigate the possibility that the crystal environment causes the strain in *S. faecalis* HPr. A 1-ns molecular dynamics simulation of *S. faecalis* HPr, under conditions that mimic the crystal environment, confirms the observations from the X-ray study, including the torsion-angle strain at residue 16. The strain disappeared, however, when *S. faecalis* HPr was simulated in a water environment, resulting in an active site configuration virtually the same as that observed in all other unphosphorylated HPrs. This indicates that the torsion-angle strain at Ala 16 in *S. faecalis* HPr is a result of crystal contacts or conditions and does not play a role in the phosphorylation–dephosphorylation cycle.

Keywords: molecular dynamics; nuclear magnetic resonance; phosphorylation; *P*-HPr; torsion-angle strain

An essential step in the transfer of carbohydrates across the cell membrane of bacteria via the phospho*enol*pyruvate-dependent phosphotransferase system (PTS; Lolkema & Robillard, 1993; Postma et al., 1993; Reizer et al., 1993) is the transfer of a phosphoryl-group from Enzyme I (EI) to HPr and its subsequent donation to Enzyme II (EII), the membrane-bound transporter. The three-dimensional structures of the unphosphorylated (Van Nuland et al., 1994) and the phosphorylated forms (Van Nuland et al., 1995) of HPr (*P*-HPr) from *Escherichia coli* have been determined by NMR and restrained molecular dynamics (rMD) refinement. In this paper, we shall compare these forms of *E. coli* HPr and discuss the consequences for HPr's function as a phosphocarrier protein.

Reprint requests to: Ruud M. Scheek, Department of Biophysical Chemistry, University of Groningen, Nijenborgh 4, 9747 AG Groningen, The Netherlands; e-mail: scheek@chem.rug.nl.

Phosphorylation-induced structural changes in HPr

Using an excess of phosphoenolpyruvate and a catalytic amount of EI, *E. coli* HPr was kept phosphorylated during the 2D ^{1}H-^{1}H NOE (NOESY) and the ^{15}N-edited 3D NOE (HSQC-NOESY) measurements. Details of the resonance assignments and the structure determination have been published (Van Nuland et al., 1995). From inspection of the ^{1}H-^{15}N correlation spectra, it was evident that the effects of His 15 phosphorylation on the structure of HPr were limited to the region around the phosphorylation site; major changes in chemical shift occurred only for the ^{1}H-^{15}N nuclei of residues His 15, Thr 16, and Arg 17. The most notable changes in NOE patterns were observed for the residues His 15 and Pro 18 as a result of the rotation of His 15 imidazole ring over a small angle away from its position perpendicular to the Pro 18 ring. This is accompanied by the introduction of unfavorable ϕ, ψ torsion angles (or

average: $\phi, \psi = 51, -119$ degrees) at His 15, in a configuration that is stabilized by an extensive hydrogen bonding network (Van Nuland et al., 1995); stable H-bonds are formed between the phosphate oxygens and the backbone amide protons of Thr 16 and Arg 17, in agreement with the large downfield chemical-shift changes and the decrease in water-exchange rates observed for these protons after phosphorylation (Rajagopal et al., 1994; Van Nuland et al., 1995). An H-bond is also present between one of the phosphate oxygens and the side chain Oγ of Thr 16. Theoretical modeling studies have correctly predicted the involvement of the amide protons of residues 16 and 17 in H-bonding to the phosphoryl group of *Bacillus subtilis* (Herzberg et al., 1992; Rajagopal et al., 1994) and *E. coli* (Rajagopal et al., 1994) *P*-HPr. Such stabilization of a phosphate by H-bonding to backbone amide protons at the N-terminus of an α-helix, as we find for *E. coli P*-HPr, has been found in several enzymes (Johnson & Barford, 1993). This arrangement is also favored by the helix macrodipole that arises from the alignment of the peptide dipoles parallel to the helix axis (Hol et al., 1978). Finally, the changes that were detected in the ϕ, ψ torsion angles of Thr 16 and Arg 17 are in agreement with the increase of the $^3J_{NHH\alpha}$-coupling constants measured for these residues in HPr and *P*-HPr (Van Nuland et al., 1995).

Figure 1A shows the differences between the active sites of *E. coli P*-HPr and the unphosphorylated HPrs from *E. coli* (Van Nuland et al., 1994) and *B. subtilis* (Herzberg et al., 1992;

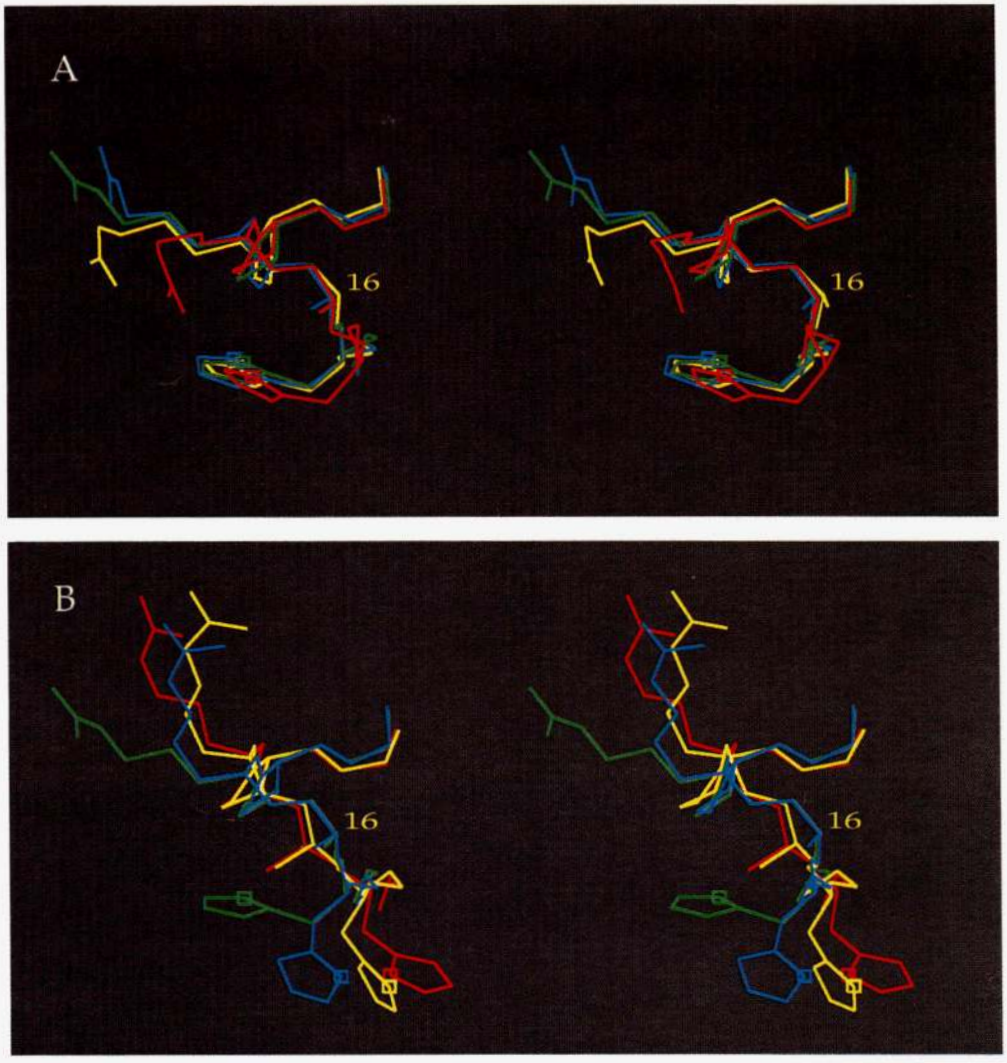

Fig. 1. Stereoscopic representation of the active site of different HPrs. The Cα atom of residue 16 is indicated. The phosphorylation site, His 15 Nδ1, is marked by an open square. The structures are superimposed such as to optimize the overlay of the backbone atoms of residues 14–19 and the side-chain atoms of Pro 18. **A:** High (PDB entry 2HPR) and low salt HPr X-ray structures of *B. subtilis* in yellow and cyan, respectively, and the structures closest to the ensemble-average of the time-averaged restrained MD trajectories of unphosphorylated (Van Nuland et al., 1994) and phosphorylated (Van Nuland et al., 1995) *E. coli* HPr in green and red, respectively. The position of the Arg 17 side chain differs in the different X-ray structures. **B:** Different *S. faecalis* HPr molecules obtained from X-ray (PDB entry 1PTF) in red, and the structures closest to the ensemble-average of the crystal MD simulation and MD simulation in water in yellow and cyan, respectively. The *E. coli* HPr NMR structure is given as reference structure in green. The torsion-angle strain at residue 16 in *S. faecalis* HPr is present during most of the crystal simulation, whereas it is released during the MD simulation in water.

Liao & Herzberg, 1994). The side chain of Arg 17 occupies a different position after phosphorylation; the $\chi 1$-angle changes from an average value of 190° to 298°, in agreement with observed $^3J_{\alpha\beta}$ and $^3J_{N\beta}$ coupling constants (Rajagopal et al., 1994). The major effect of the sulphate ion in the high-salt X-ray structure of *B. subtilis* HPr (Herzberg et al., 1992) seems to be a reorientation of the Arg 17 side chain, away from the more extended configuration seen in the low-salt X-ray structure of *B. subtilis* HPr and in the solution structure of *E. coli* HPr. The configuration of the active site of *E. coli P*-HPr shown in Figure 1A, with strain in the backbone torsion angles of residue 15, does not change significantly during a further 350 ps of unrestrained MD simulation, which we performed after the rMD refinement (on average: $\phi,\psi = 29,-125$ degrees).

X-ray studies of HPr: Torsion-angle strain in unphosphorylated HPr?

Jia et al. (1993b; 1994) have presented evidence of torsion-angle strain at residue 16 in unphosphorylated *Streptococcus faecalis* HPr. When they compared the X-ray structure of this protein with that of *B. subtilis* HPr (Herzberg et al., 1992), which lacks this strain, they noted that a sulphate ion had cocrystallized in the active site of *B. subtilis* HPr. They proposed that the differences between the two X-ray structures reflect the conformational changes that occur during a phosphorylation/dephosphorylation cycle, assuming that the sulphate can be seen as a phosphate analogue. In their view, the imidazole ring of His 15 and the side chain of Arg 17 cycle between different relative positions according to the phosphorylation state of the protein and the strain at residue 16 is released upon phosphorylation. This model of HPr's mode of action predicts that torsion-angle strain should be observable in other unphosphorylated HPrs as well. However, in none of the structures of HPr that have been solved since this model was proposed (Herzberg et al., 1992; Wittekind et al., 1992; Jia et al., 1993a; Kalbitzer & Hengstenberg, 1993; Liao & Herzberg, 1994; Van Nuland et al., 1994; 1995) has there been any indication of torsion-angle strain at residue 16. Most notably, another X-ray study of *B. subtilis* HPr (Liao & Herzberg, 1994), which lacked cocrystallized sulphate near His 15, showed no strain at residue 16. As shown in Figure 1A, the major effect of the presence of a sulphate ion in the active site of *B. subtilis* HPr seems to be a reorientation of the Arg 17 side chain, away from the more extended configuration in the absence of the sulphate ion and in the solution structure of *E. coli* HPr. These observations have led us to question whether the torsion-angle strain at residue 16 in the X-ray structure of *S. faecalis* HPr is an artefact of the crystal conditions.

Results and discussion

MD simulations S. faecalis HPr

In order to investigate the possibility that the crystal environment is responsible for the torsion-angle strain in *S. faecalis* HPr, we performed a MD simulation of the protein *in a crystal*. Four molecules of HPr, comprising one unit cell, were simulated independently. They were surrounded by the crystal-water molecules, additional water molecules to arrive at the appropriate density, and sodium ions to compensate for the net charge of the protein. We used periodic boundary conditions to further mimic the crystal periodicities. After equilibration, we continued the MD simulation for 1 ns. Figure 2 shows the RMS Cα-positional differences between the X-ray structure and snapshots from the MD simulation. On average, these differences do not exceed 0.11 nm for the four HPr molecules. Peaks in the Cα RMS fluctuations during the MD simulation correspond to peaks in the *B*-factors of these atoms, although the quantitative agreement was poor. Many of the Cα fluctuations seen during the MD simulation were significantly larger than those predicted from the corresponding *B*-factors. Nevertheless, the torsion-angle strain at Ala 16 is remarkably stable, as shown in Figure 3. It persists throughout the MD simulation for two of the four HPr molecules, whereas the other two molecules are able to adopt relaxed conformations during some periods of the MD simulation. On average, the simulated ϕ,ψ angles of Ala 16 are close to those observed in the crystal structure. This persistence of the Ala 16 torsion-angle strain in the crystal MD simulation must be contrasted to its behavior in a 0.5-ns solvent MD simulation of one molecule of *S. faecalis* HPr in a water environment (Fig. 4); almost immediately after this solvent simulation was started, the protein backbone in the active site rearranged, releasing the Ala 16 torsion-angle strain. During the remainder of the solvent simulation, the active site loop had virtually the same configuration as that observed in all other unphosphorylated HPrs (see Fig. 1B). We conclude that the crystal environment is indeed responsible for the backbone torsion-angle strain

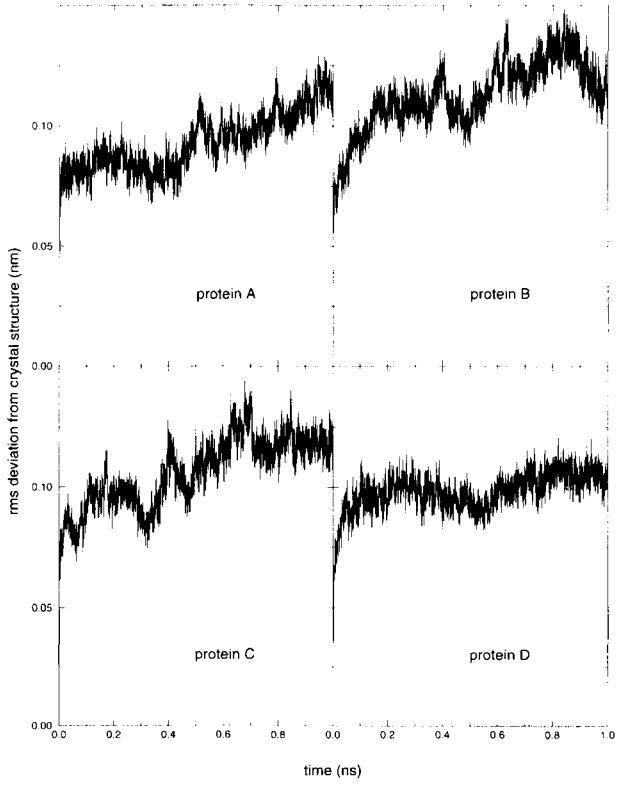

Fig. 2. Cα-positional RMS differences calculated for each of the four simulated HPr molecules (labeled A–D) with respect to the crystal Cα coordinates during the 1-ns MD simulation of crystalline *S. faecalis* HPr. Averaged over the total MD simulation and all four HPr molecules, the RMS difference with respect to the X-ray structure is 0.10 nm.

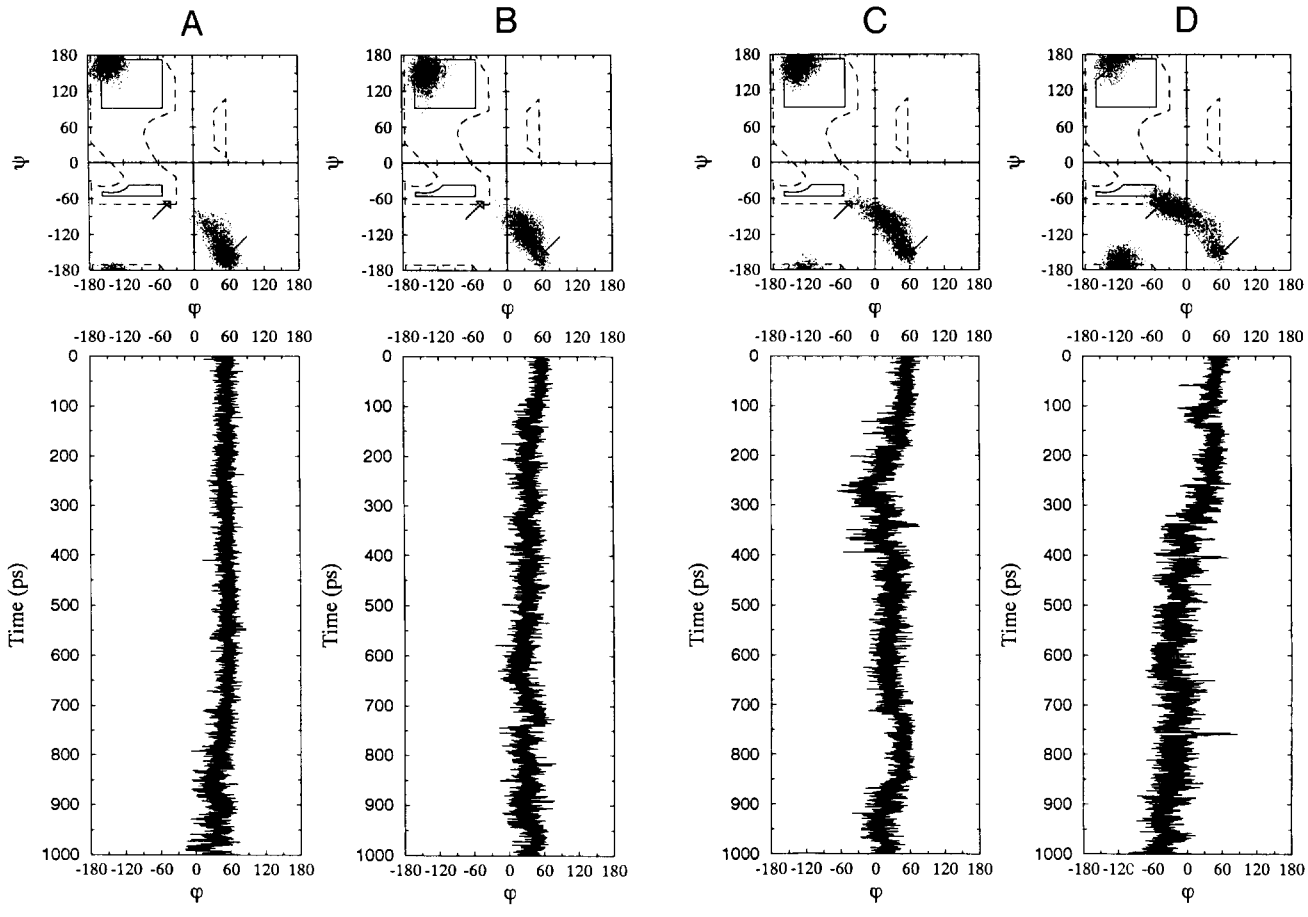

Fig. 3. ϕ,ψ Torsion angles of residues 15 and 16, monitored during the 1-ns crystal MD simulation of *S. faecalis* HPr given for all four molecules (labeled A–D) in the simulated unit cell. The upper part corresponds to the Ramachandran plot (Ramachandran et al., 1963), with His 15 and Ala 16 ϕ,ψ values indicated by dots taken every 0.2 ps. Arrows point to the Ala 16 ϕ,ψ values found in the crystal (right lower) and the averaged value calculated from the solution MD simulation of HPr (left upper, see Fig. 4). The lower part shows the ϕ torsion-angle fluctuation of Ala 16 during the 1-ns MD simulation for molecules A, B, C, and D. **A,B:** The torsion-angle strain persists during the 1-ns simulation in molecule. **C,D:** The torsion-angle strain fluctuates between the strained and unstrained configuration.

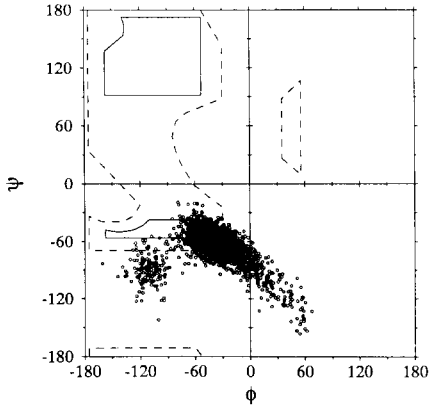

Fig. 4. ϕ,ψ Torsion angles of residue 16, monitored during the 0.5-ns solution MD simulation of *S. faecalis* HPr. Ramachandran plot showing the Ala 16 ϕ,ψ values during the solution MD simulation of *S. faecalis* HPr, indicated by dots taken every 0.2 ps. These torsion angles relax immediately after the start of the MD simulation and no strain is observed during the remainder of the simulation.

at residue 16 in *S. faecalis* HPr. A comparable situation was observed by Liao and Herzberg (1994) for residue 30 in two different crystal forms of *B. subtilis* HPr; here differences in the crystal environment caused significantly different backbone torsion angles for this residue.

Conclusions

We have shown that the torsion-angle strain in the unphosphorylated form of *S. faecalis* HPr is caused by crystal conditions and is not present in solution. On the other hand, we did find strain in the backbone torsion angles of the phosphorylated His 15 of *E. coli P*-HPr, by NMR and rMD refinement. Speculations about the precise role of this strain in the phosphoryl-transfer from HPr to Enzyme II are premature until we know the structure of the phosphorylated complex of HPr and Enzyme II. As a technical point, we note that MD simulations of a protein in crystal and solvent environments have proven to be a valuable tool for assessing the validity of such detailed conclusions from X-ray and NMR structure determinations.

Materials and methods

The protocol used for the time-averaged distance-restrained MD simulations in water at 300 K on *E. coli* HPr and *P*-HPr has been described in detail previously (Van Nuland et al., 1994, 1995). The charge distribution for the unphosphorylated and phosphorylated imidazole ring were calculated ab initio and converted into appropriate GROMOS charges (Van Nuland et al., 1995).

In the X-ray study of *S. faecalis* HPr, no density was found for the side chain of Lys 83 and for the C-terminal Glu 88. We replaced Ala 83 by a lysine, as in the wild-type protein, and added the C-terminal glutamate. The initial unit cell configuration was generated as follows. Symmetry related copies of *S. faecalis* were obtained by applying P21212 transformations on the starting structure. The structure was solvated, and subjected to 100 steps of energy-minimization (EM) with position restraints (force constant 1,000 $kJ \cdot mol^{-1} \cdot nm^{-2}$) on the protein atoms and the 396 crystal waters using the GROMACS (Bekker et al., 1993; Van der Spoel, 1995) suite of programs with the 37C4 force field parameters (Van Gunsteren & Berendsen, 1987). We used periodic boundary conditions to further mimic the crystal environment. Fifty extra water molecules were inserted to approach the experimental solvent content of 36% (v/v) and allowed to equilibrate during 5 ps of position restrained MD. To compensate for a total net charge of −20, 20 solvent molecules were replaced by sodium ions at positions with the lowest electrical potential (the potential was reevaluated after each ion insertion). The system was energy-minimized by another 100 steps of position-restrained EM. Finally, a unit cell was obtained with 4 proteins, 20 sodium ions, and 826 solvent molecules, with cell dimensions $5.356 \times 4.546 \times 2.988$ nm^3. The calculated solvent content was 34% (v/v). This system was subjected to 25 ps of position-restrained MD, followed by 1 ns of free MD. An integration time step of 1 fs was used. Nonbonded interactions were evaluated within a cut-off radius of 1.4 nm. The system was anisotropically pressure-coupled to a reservoir of 1 bar (time-constant 0.5 ps) and temperature-coupled to a reservoir of 287 K (time-constant 0.05 ps; Berendsen et al., 1984). During the 1-ns simulation, the cell-dimensions remained constant and within 3% from the experimental value. The 1-ns crystal MD simulation took 270 CPU hours on a GROMACS1 (Bekker et al., 1993) computer using 22 processors.

The same *S. faecalis* HPr X-ray structure was used to start an MD simulation in water. The protein was solvated in a cubic box containing 2,608 water molecules, including the 99 crystal waters. After 100 steps of steepest-descent EM, a 20-ps MD simulation was started, using position restraining with a force constant of 1,000 $kJ \cdot mol^{-1} \cdot nm^{-2}$. After this equilibration period, the simulation was continued for 500 ps while isotropically pressure coupled. The temperature of the system was kept at 287 K by coupling to a temperature bath with a relaxation time of 0.05 ps. Nonbonded interactions were evaluated using a cut-off radius of 1.0 nm and an integration time step of 1 fs was used. Other details are as described previously (Van Nuland et al., 1995).

Acknowledgments

This research was supported by the Netherlands Foundation for Chemical Research (SON) with financial aid from the Netherlands Organisation for Scientific Research (NWO). The SNARF program, written by FRANS van Hoesel, was used for processing, visualizing, and analyzing all NMR data sets. We thank Dr. Osnat Herzberg for providing us with the low salt X-ray *B. subtilis* HPr coordinates.

References

Bekker H, Berendsen HJC, Dijkstra EJ, Achterop S, Van Drunen R, Van der Spoel D, Sijbers A, Keegstra H, Reitsma B, Renardus MKR. 1993. Gromacs: A parallel computer for molecular dynamics simulations. In: de Groot RA, Nadrchal J, eds. *Physics computing 92*. Singapore: World Scientific. pp 252–256.

Berendsen HJC, Postma JPM, Van Gunsteren WFG, DiNola A, Haak JR. 1984. Molecular dynamics with coupling to an external bath. *J Chem Phys 81*:3684–3690.

Herzberg O, Reddy P, Sutrina S, Saier MH, Reizer J, Kapafia G. 1992. Structure of the histidine-containing phosphocarrier protein HPr from *Bacillus subtilis* at 2.0 Å resolution. *Proc Natl Acad Sci USA 89*:2499–2503.

Hol WGJ, Van Duijnen PTh, Berendsen HJC. 1978. The α-helix dipole and the properties of proteins. *Nature 273*:443–446.

Jia Z, Quail JW, Waygood EB, Delbaere LTJ. 1993a. The 2.0-Å resolution structure of *Escherichia coli* histidine-containing phosphocarrier protein HPr. *J Biol Chem 268*:22490–22501.

Jia Z, Vandonselaar M, Hengstenberg W, Quail JW, Delbaere LTJ. 1994. The 1.6-Å structure of histidine-containing phosphotransfer protein HPr from *Streptococcus faecalis*. *J Mol Biol 236*:1341–1355.

Jia Z, Vandonselaar M, Quail JW, Delbaere LTJ. 1993b. Active-centre torsion-angle strain revealed in 1.6 Å-resolution structure of histidine-containing phosphocarrier protein. *Nature 361*:94–97.

Johnson LN, Barford D. 1993. The effects of phosphorylation on the structure and function of proteins. *Annu Rev Biophys Biomol Struct 22*: 199–232.

Kalbitzer HR, Hengstenberg W. 1993. The solution structure of the histidine-containing protein (HPr) from *Staphylococcus aureus* as determined by two-dimensional ^{1}H-NMR spectroscopy. *Eur J Biochem 216*:205–214.

Liao DI, Herzberg O. 1994. Refined structures of the active Ser 83-Cys and impaired Ser 46-Asp histidine-containing phosphocarrier proteins. *Structure 2*:1203–1216.

Lolkema JS, Robillard GT. 1993. The enzyme II of the phosphoenolpyruvate-dependent carbohydrate transport systems. In: de Pont JJHHM, ed. *The new comprehensive biochemistry : Pumps, carriers and channels*. Amsterdam: Elsevier/North Biomedical Press. pp 135–167.

Postma PW, Lengeler JW, Jacobson GR. 1993. Phosphoenolpyruvate: Carbohydrate phosphotransferase system of bacteria. *Microbiol Rev 57*: 543–594.

Rajagopal P, Waygood EB, Klevit RE. 1994. Structural consequences of histidine phosphorylation: NMR characterization of the phosphohistidine form of histidine-containing protein from *Bacillus subtilis* and *Escherichia coli*. *Biochemistry 33*:15271–15282.

Ramachandran GN, Ramakrishnan C, Sasisekharan V. 1963. Stereochemistry of polypeptide chain configurations. *J Mol Biol 7*:95–99.

Reizer J, Hoischen C, Reizer A, Pham TN, Saier MH. 1993. Sequence analyses and evolutionary relationships among the energy-coupling proteins Enzyme I and HPr of the bacterial phosphoenolpyruvate:sugar phosphotransferase system. *Protein Sci 2*:506–521.

Van der Spoel D. 1995. *Gromacs user manual*. Groningen, The Netherlands: Biomos.

Van Gunsteren WF, Berendsen HJC. 1987. *GROningen MOlecular Simulation (GROMOS) library manual*. Groningen, The Netherlands: Biomos.

Van Nuland NAJ, Boelens R, Scheek RM, Robillard GT. 1995. The high-resolution structure of the phosphorylated form of the histidine-containing phosphocarrier protein HPr from *Escherichia coli* determined by restrained molecular dynamics from NMR-NOE data. *J Mol Biol 246*: 180–193.

Van Nuland NAJ, Hangyi IW, Van Schaik RC, Berendsen HJC, Van Gunsteren WF, Scheek RM, Robillard GT. 1994. The high-resolution structure of the the histidine-containing phosphocarrier protein HPr from *Escherichia coli* determined by restrained molecular dynamics from nuclear magnetic resonance nuclear Overhauser effect data. *J Mol Biol 237*: 544–559.

Wittekind M, Rajagopal P, Branchini BR, Reizer R, Saier MH, Klevit RE. 1992. Solution structure of the phosphocarrier protein HPr from *Bacillus subtilis* by two-dimensional NMR spectroscopy. *Protein Sci 1*:1363–1376.